Letter to the Editor

Immunologic reconstitution following hematopoietic stem cell transplantation despite lymph node paucity in NF-κB–inducing kinase deficiency

To the Editor:

Antigen-specific adaptive immunity requires interactions between T cells, B cells, and dendritic cells in secondary lymphoid organs, which include tonsils, lymph nodes (LNs), Peyer patches, and splenic follicles. Activation of the noncanonical nuclear factor kappa B (NF-κB) pathway in stromal cells following lymphotoxin β receptor (LTβR) ligation by $LT\alpha_1\beta_2$ expressed on lymphoid inducer cells is critical for lymphorganogenesis, whereas its activation in B cells after B-cell activating factor receptor ligation is important for survival.[1] LTβR ligation drives NF-κB–inducing kinase (NIK) to phosphorylate inhibitor of NF-κB kinase subunit alpha.[1] Inhibitor of NF-κB kinase subunit alpha subsequently phosphorylates NF-κB2/p100, which contains an IκB-like domain that prevents nuclear translocation of the p100:RelB complex.[1] Phosphorylated p100 undergoes polyubiquitination and proteasomal processing to p52.[1] p52:RelB dimers translocate to the nucleus and activate the transcription of genes encoding chemokines and adhesion molecules for lymphorganogenesis, including *VCAM1* and chemokine (C-C motif) ligand 20.[2] $NIK^{-/-}$ and $NIK^{Gy860Arg/Gy860Arg}$ (*aly/aly*) mice have absent LNs, B-cell lymphopenia, disrupted splenic architecture, and hypogammaglobulinemia.[3,4] Because p100 is under the transcriptional control of the classical NF-κB pathway, activating missense mutations in IκBα disrupt both classical and nonclassical NF-κB signaling pathways.[5] Consequently, lymphorganogenesis is severely impaired, hematopoietic stem cell transplantation (HSCT) fails to achieve immunologic reconstitution, despite excellent donor cell chimerism, and recurrent infections and need for immunoglobulin replacement persist after HSCT.[5] Two homozygous mutations in NIK, $NIK^{pro565Arg}$, and $NIK^{Val344Met}$ have been described in 3 patients from 2 kindreds, who lacked tonsils and palpable LNs.[6,7] The only transplanted patient was reported to be well, but no information on immune function was provided.[6] We document robust immunologic reconstitution post-HSCT in an NIK-deficient patient with abrogation of noncanonical NF-κB signaling, absence of tonsils, and paucity of LNs, and we discuss why HSCT may successfully treat NIK deficiency.

Patient 1 (P1), born to consanguineous parents (Fig 1, *A*), presented at age 1 year with recurrent sinopulmonary and gastrointestinal infections and *Candida lusitaniae* oral infections. He had panhypogammaglobulinemia (IgG < 30 mg/dL; IgM < 8 mg/dL; IgA < 4 mg/dL), undetectable antibody response to tetanus vaccination. He was started on intravenous immunoglobulin replacement and sulfamethoxazole/trimethoprim prophylaxis. At 18 months, he developed a seizure with multiple ring-enhancing lesions in the bilateral cerebral cortexes. Brain biopsy was positive for Mycobacterium, with antimicrobial resistance profile characteristic of BCG he had been vaccinated with. He was treated with antimycobacterial therapy and prednisone and referred at age 30 months to Boston Children's Hospital.

Physical examination revealed short stature (<third percentile), absent tonsils, and no palpable LNs. He had a normal total lymphocyte count, B-cell lymphopenia, and severely reduced percentages of $CD45RO^+$ memory T cells and IgD^-CD27^+ switched memory B cells (Table I). T-cell proliferation was normal to PHA, and modestly reduced to tetanus and Candida antigens (Table I). TLR responses, including TNF-α production, were normal (see Fig E1 in this article's Online Repository at www.jacionline.org), and serum TNF-α level was elevated (41 pg/mL). Biopsy of a draining axillary LN was attempted after tetanus reimmunization, but no LNs were identified. To our surprise, lymphoscintigraphy of the lower limb visualized a few right popliteal LNs, but no inguinal LNs (see Fig E2 in this article's Online Repository at www.jacionline.org), leading us to pursue HSCT. Nineteen months after antimycobacterial therapy, he demonstrated radiological improvement of brain lesions, and underwent HSCT from an HLA-matched related donor preceded by myeloablative conditioning with busulfan and fludarabine. A year post-HSCT, he is well and demonstrates robust engraftment (>95%) of all hematopoietic lineages. Importantly, he has normal B-cell count, normal IgG level, robust pneumococcal and tetanus antibody responses, and strong T-cell proliferation to tetanus after vaccination. Tonsils and LNs remained undetectable on physical examination. Norovirus in the stools and oral Candida infection cleared post-HSCT. There was no evidence of cytomegalovirus or EBV infections before, during, and after HSCT. P2, P3, and P4 are cousins of P1 (Fig 1, *A*). They all have recurrent sinopulmonary infections, bronchiectasis, chronic diarrhea with no pathogens isolated, oral thrush, undetectable tonsils and LNs, and normal lymphocyte and T-cell counts. P3 and P4 have B-cell lymphopenia. They all have hypogammaglobulinemia and have been placed on intravenous immunoglobulin replacement. HSCT has been declined by their parents.

Whole-exome sequencing of P1, P2, and P3 revealed a homozygous frameshift mutation in *MAP3K14* encoding NIK (c.916delT:p.Cys306Valfs*2) within the single region of homozygosity shared by the patients. Sanger sequencing of genomic DNA confirmed the presence of the mutation in all probands (see Fig E3 in this article's Online Repository at www.jacionline.org). The parents of P1 were heterozygous for the mutation. The frameshift mutation results in substitution of the Cys^{306} residue with valine, followed by 2 novel residues and a premature stop codon (Fig 1, *C*). The patient fibroblasts had significantly lower *NIK* mRNA levels than those of controls (Fig 1, *D*). Because endogenous NIK protein level is extremely low due to continuous degradation by TNF Receptor Associated Factor 3,[2] expression of an N-terminal Myc-tagged mutant NIK was examined in transfected HEK293T cells. Immunoblotting revealed an approximately 130-kDa band in wild-type NIK-transfected cells and an approximately 34-kDa band in $NIK^{Cys306Valfs*2}$-transfected cells, corresponding to the expected sizes of wild-type and mutant NIK (Fig 1, *E*). Fibroblasts from P1 stimulated with α-LTβR for 48 hours had absent p100 phosphorylation and processing (Fig 1, *F*). P1 fibroblasts also failed to upregulate *VCAM1* and chemokine (C-C motif) ligand 20 expression after α-LTβR stimulation but did so normally after TNF-α stimulation (Fig 1, *G*).
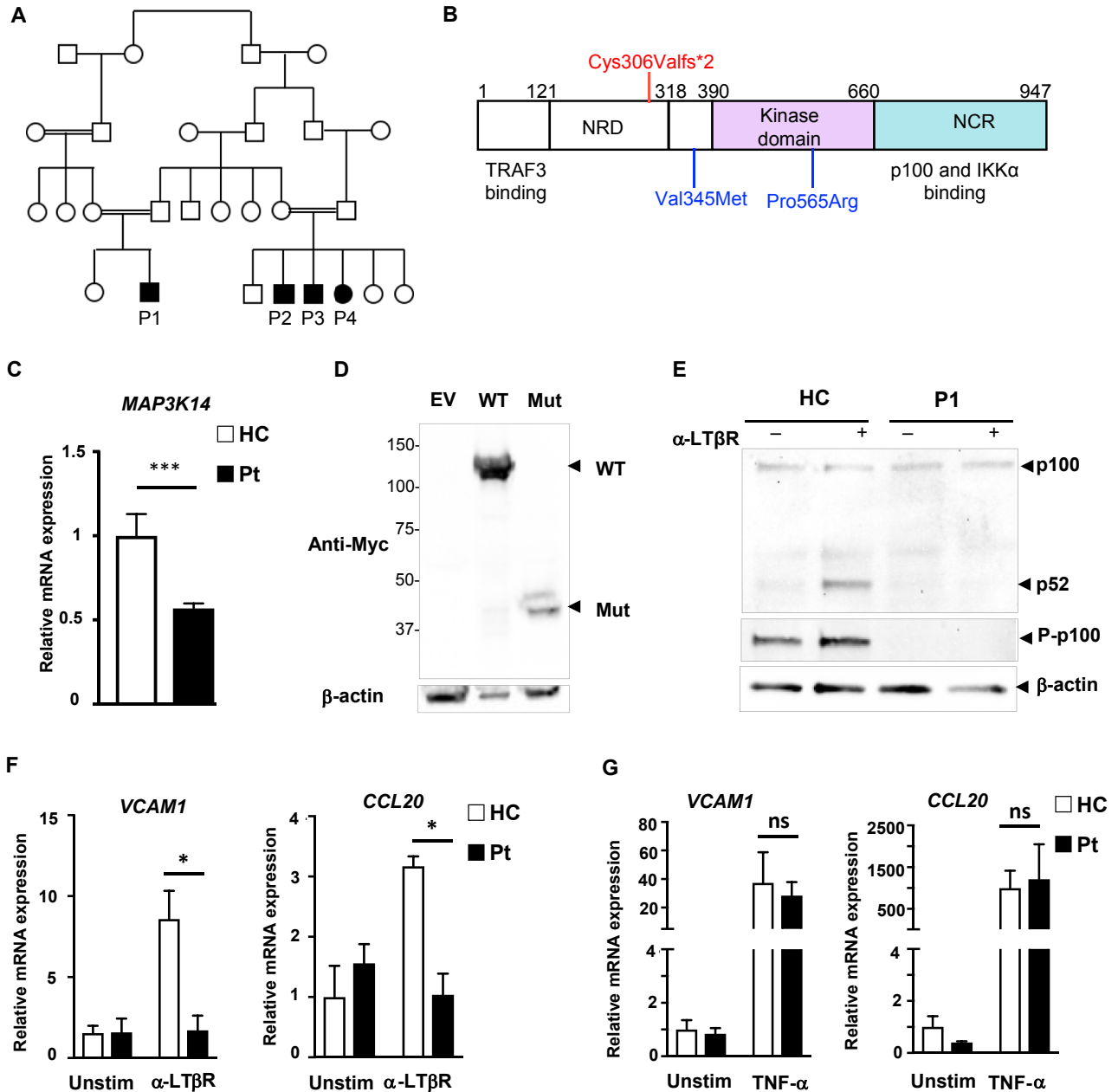
FIG 1. The NIK Cys306Valfs*2 mutation and its impact on signaling. **A,** Family pedigree. **B,** Linear map of NIK. The mutation in our patients is indicated in red, and in the 2 reported kindreds in blue. **C,** *MAP3K14* mRNA expression in fibroblasts from P1 and a healthy control (HC). Data are representative of 3 independent experiments. **D,** NIK Protein expression in 293T cells transfected with WT NIK^{myc} or mutated (mut) NIK^{myc}. **E,** p100 processing and phosphorylation in unstimulated (unstim) and α-LTβR–stimulated fibroblasts from P1 and HC. Similar data were obtained in 2 independent experiments. **F** and **G,** *VCAM1* and *CCL20* mRNA expression in unstimulated and anti–LTβR-stimulated (Fig 1, *F*) and unstimulated and TNF-α–stimulated (Fig 1, *G*) fibroblasts from P1 and HC. Data are representative of 3 independent experiments. Columns and bars represent the mean ± SEM. *CCL20,* Chemokine (C-C motif) ligand 20; *EV,* empty vector; *Pt,* patient; *WT,* wild-type. *$P < .05$, **$P < .01$, and ***$P < .001$.

Lymphotoxin α can drive the formation of mesenteric and cervical LNs, and splenic PNA$^+$ B-cell clusters independently from LTβR signaling in $LTβ^{-/-}$ mice.[8] Increased TNF-α levels can drive mesenteric LNs and organized spleen formation in the absence of LTβR.[9] Intact lymphotoxin α and TNF-α production and signaling, which depend on the classical NF-κB pathway, may have permitted residual lymphoid structures to form in our patient, also reflected in his lack of lymphocytosis and near-normal antigen-specific T-cell proliferation studies. Residual secondary lymphoid organs (SLOs) may have enabled

TABLE I. Immunologic profiles of the patients

Parameter	P1 Pre-HSCT (3.5 y)	P1 Post-HSCT (5.5 y)	P2 (20 mo)	P3 (5 y)	P4 (8 y)
		Patient age at the time of testing			
Lymphocyte subsets					
CD3$^+$ (10^3 cells/μL)	4.44 (0.85-4.6)	3.01 (0.77-4.0)	3.727 (1.4-7.2)	**5.53** (0.85-4.6)	3.77 (0.77-4.0)
CD3$^+$CD4$^+$ (10^3 cells/μL)	**3.15** (0.7-2.7)	1.57 (0.4-2.5)	3,359 (0.8-5.2)	**4.57** (0.7-2.7)	**2.77** (0.4-2.5)
CD45RA$^+$CCR7$^+$ (% CD4$^+$)	**91.3** (65.2-84.8)	**56.3** (57.1-84.8)	**91.7** (66.3-89)	**88.8** (57.1-84.8)	**86** (57.1-84.8)
CD45RA$^+$CCR7$^-$ (% CD4$^+$)	0.1 (0.2-3)	1.3 (0.4-2.6)	1.43 (0.2-2.9)	1.12 (0.4-2.6)	1.43 (0.4-2.6)
CD45RA$^-$CCR7$^+$ (% CD4$^+$)	**6.65** (10.5-23.2)	23.5 (11.2-26.7)	3.79 (1.3-9.4)	**3.23** (11.2-26.7)	**4.53** (11.2-26.7)
CD45RA$^-$CCR7$^-$ (% CD4$^+$)	**2.1** (2.9-9.8)	18.8 (3.3-15.2)	3.11 (3-9.4)	**6.89** (3.3-15.2)	8.08 (3.3-15.2)
CD3$^+$CD8$^+$ (10^3 cells/μL)	1.23 (0.49-1.3)	**1.39** (0.49-1.3)	0.475 (0.2-2.8)	0.99 (0.49-1.3)	0.974 (0.49-1.3)
CD45RA$^+$CCR7$^+$ (% CD8$^+$)	**96.6** (39-89)	**14** (28.4-80)	67 (66-89)	**84** (28.4-80)	**90.4** (28.4-80)
CD45RA$^+$CCR7$^-$ (% CD8$^+$)	1 (4.8-30)	13.9 (9.1-49.1)	**29.3** (6.4-20.8)	12.7 (9.1-49.1)	**4.31** (9.1-49.1)
CD45RA$^-$CCR7$^+$ (% CD8$^+$)	1 (0.9-5.7)	**16.6** (1-4.5)	2.74 (1.7-8.5)	**1.49** (1-4.5)	1.28 (1-4.5)
CD45RA$^-$CCR7$^-$ (% CD8$^+$)	**1.4** (3.4-28.2)	**55.8** (6.2-29.3)	**1.02** (5.1-25.1)	**0.86** (6.2-29.3)	**3.89** (6.2-29.3)
CD19$^+$ (10^3 cells/μL)	**0.333** (0.39-1.4)	0.752 (0.39-1.4)	0.61 (0.16-3.7)	**0.238** (0.39-1.4)	**0.145** (0.39-1.4)
CD27$^-$IgD$^+$ (% CD19$^+$)	**95.11** (54-88.4)	**96.1** (54-88.4)	**91.7** (68-89)	**91.5** (54-88.4)	**90.1** (47-77)
CD27$^+$IgD$^+$ (% CD19$^+$)	**1.4** (2.7-19.8)	**0.8** (2.7-19.8)	**1.85** (4.1-13.9)	**0.77** (2.7-19.8)	**1.49** (5.2-20.4)
CD27$^+$IgD$^-$ (% CD19$^+$)	**1.8** (3.3-7.4)	**2.4** (3.3-7.4)	**0.71** (3.9-13.6)	**1.16** (3.3-7.4)	**1.49** (10.9-30.4)
CD3$^-$CD56$^+$ (10^3 cells/μL)	**0.045** (0.13-0.72)	**1.46** (0.13-0.72)	0.222 (0.1-0.8)	0.281 (0.13-0.72)	0.261 (0.13-0.72)
Proliferation (control)					
PHA	278,399 (187,403)	123,764 (173,788)	64,091 (45,243)	30,206 (22,965)	20,268 (22,965)
Tetanus toxoid	12,998 (18,084)	100,043 (26,480)	ND	ND	ND
Candida	20,084 (35,821)	209,546 (37,857)	ND	ND	ND
Immunoglobulins	**(1 y)**	**(5.5 y)**	**(20 mo)**	**(1 y)**	**(4 y)**
IgG (mg/dL)	**<30**	973	**<200**	**<30**	**228**
IgM (mg/dL)	**10**	75	**<30**	68	**32**
IgA (mg/dL)	**<5**	**16**	**<5**	**<5**	**<5**
Tetanus vaccine titer	ND	1.13	ND	ND	ND

The values in parentheses for proliferation are those obtained on PBMCS from a normal healthy control studied in parallel and on the same day as patients. The boldface values represent an abnormal value.

ND, Not done; *UD*, undetectable.

donor hematopoietic cells to mount a robust adaptive immune response in our patient. As in our patient, HSCT corrects low serum IgG levels in *aly/aly* mice.[3] In contrast, in patients and mice with missense mutations in IκBα, disruption of both classical and noncanonical NF-κB signaling results in both impaired TNF-α production and defective LTβR signaling, which may not allow the formation of sufficient SLOs for the development of an adaptive immune response, resulting in failure of HSCT to achieve immune reconstitution. HSCT may be useful in treating patients with NIK deficiency, or other deficiencies that selectively disrupt the noncanonical NF-κB pathway, who have residual SLOs.

Khaoula Ben Farhat, PhD[a]*
Mohammed F. Alosaimi, MD[a,b]*
Hiba Shendi, MBBS[c]
Suleiman Al-Hammadi, MBBS[d]
Jennifer Jones, BA[a]
Klaus Schwarz, MD[e]
Ansgar Schulz, MD[f]
Laila S. Alawdah, MBBS[g]
Sandra Burchett, MD, MSc[g]
Sultan Albuhairi, MD[a]
Jennifer Whangbo, MD, PhD[h]
Neha Kwatra, MBBS[i]
Hanan E. Shamseldin, MSc[j]
Fowzan S. Alkuraya, MD[j]
Janet Chou, MD[a]‡
Raif S. Geha, MD[a]‡

From [a]the Division of Immunology, Boston Children's Hospital and Harvard Medical School, Boston, Mass; [b]the Department of Pediatrics, King Saud University, Riyadh, Saudi Arabia; [c]the Department of Allergy/Immunology, Tawam Hospital, Al Ain, United Arab Emirates; [d]the Department of Pediatrics, College of Medicine and Health Sciences, UAE University, Al Ain, United Arab Emirates; [e]the Institute for Transfusion Medicine, Ulm University and Institute for Clinical Transfusion Medicine and Immunogenetics Ulm, German Red Cross Blood Service Baden-Württemberg – Hessen, Ulm, Germany; [f]the Department of Pediatrics and Adolescent Medicine, University Medical Center, Ulm, Germany; [g]the Division of Infectious Diseases, Boston Children's Hospital, Harvard Medical School, Boston, Mass; [h]the Division of Pediatric Hematology-Oncology, Boston Children's Hospital and the Dana Farber Cancer Institute, Boston, Mass; [i]the Division of Nuclear Medicine, Boston Children's Hospital, Harvard Medical School, Boston, Mass; and [j]the Department of Genetics, King Faisal Specialist Hospital and Research Center, Riyadh, Saudi Arabia. E-mail: Mohammed.Alosaimi@childrens.harvard.edu.

*Equal contributing first authors.

‡Equal contributing last authors.

REFERENCES
1. Sun SC. The non-canonical NF-kappaB pathway in immunity and inflammation. Nat Rev Immunol 2017;17:545-58.
2. van de Pavert SA, Mebius RE. New insights into the development of lymphoid tissues. Nat Rev Immunol 2010;10:664-74.
3. Miyawaki S, Nakamura Y, Suzuka H, Koba M, Yasumizu R, Ikehara S, et al. A new mutation, aly, that induces a generalized lack of lymph nodes accompanied by immunodeficiency in mice. Eur J Immunol 1994;24:429-34.
4. Yin L, Wu L, Wesche H, Arthur CD, White JM, Goeddel DV, et al. Defective lymphotoxin-beta receptor-induced NF-kappaB transcriptional activity in NIK-deficient mice. Science 2001;291:2162-5.

5. Petersheim D, Massaad MJ, Lee S, Scarselli A, Cancrini C, Moriya K, et al. Mechanisms of genotype-phenotype correlation in autosomal dominant anhidrotic ectodermal dysplasia with immune deficiency. J Allergy Clin Immunol 2018;141:1060-73.e3.

6. Willmann KL, Klaver S, Dogu F, Santos-Valente E, Garncarz W, Bilic I, et al. Biallelic loss-of-function mutation in NIK causes a primary immunodeficiency with multifaceted aberrant lymphoid immunity. Nat Commun 2014;5:5360.

7. Schlechter N, Glanzmann B, Hoal EG, Schoeman M, Petersen BS, Franke A, et al. Exome sequencing identifies a novel MAP3K14 mutation in recessive atypical combined immunodeficiency. Front Immunol 2017;8:1624.

8. Alimzhanov MB, Kuprash DV, Kosco-Vilbois MH, Luz A, Turetskaya RL, Tarakhovsky A, et al. Abnormal development of secondary lymphoid tissues in lymphotoxin beta-deficient mice. Proc Natl Acad Sci U S A 1997;94: 9302-7.

9. Furtado GC, Pacer ME, Bongers G, Benezech C, He Z, Chen L, et al. TNFα-dependent development of lymphoid tissue in the absence of RORγt(+) lymphoid tissue inducer cells. Mucosal Immunol 2014;7: 602-14.

METHODS
Patients
All study participants were recruited using written informed consent approved by the respective institutional review boards.

Whole-exome sequencing and Sanger sequencing
Whole-exome sequencing was performed on 3 probands from 2 related kindreds as described.[E1] Sanger sequencing was used to validate the identified mutation in the probands and verify the carrier status of the parents as described.[E1]

Cell lines
Skin fibroblast cell lines were established for P1 and a healthy control as described.[E1] HEK293 T cells and primary skin fibroblasts were grown in Dulbecco modified Eagle medium (Gibco, Waltham, Mass) supplemented with 10% FBS (Gibco), 50,000 IU penicillin (Lonza, Basel, Switzerland), 50,000 μg streptomycin (Lonza), 10 μM HEPES (Gibco), and 2 mM glutamine (Lonza).

Fibroblast stimulation
At about 80% confluency, fibroblasts were trypsinized and reseeded at a density of 100,000 cells per well (6-well format). For quantitative RT-PCR analysis, fibroblasts were treated with 5 μg/mL of LEAF antihuman lymphotoxin beta receptor (α-LTβR) (Clone 31G4D8; Biolegend, San Diego, Calif) for 48 hours or with 10 ng/mL TNF-α (210-TA; R&D Systems, Minneapolis, Minn) for 6 hours. For immunoblot analysis, fibroblasts were treated with 5 μg/mL (α-LTβR) for 48 hours with addition of the proteasome inhibitor (MG132) (474791; Calbiochem, San Diego, Calif) at a final concentration of 10 μM in the last 5 hours.

Quantitative real-time PCR analysis
Total RNA was isolated from fibroblasts using RNeasy Mini Kit (Qiagen, Venlo, The Netherlands) according to the manufacturer's instructions. For each sample, cDNA was generated from 200 ng of RNA in a total volume of 20 μL using the iScript cDNA synthesis kit (Bio-Rad Laboratories, Hercules, Calif). Real-time PCR was performed with TaqMan Fast Advanced Master Mix (Applied Biosystems, Beverly Hills, Calif). Experiments were run on a QuantStudio 3 Real-Time PCR System (Applied Biosystems). TaqMan probes for human *MAP3K14*, *VCAM1*, chemokine (C-C motif) ligand 20, and glyceraldehyde-3-phosphate dehydrogenase were purchased from Thermo Fisher Scientific (Waltham, Mass). Data were analyzed by using the $2^{-\Delta Ct}$ method after normalization to *glyceraldehyde-3-phosphate dehydrogenase* gene as an endogenous control.

Mutagenesis and transfection
Targeted mutagenesis was performed using the QuikChange II XL Site-Directed Mutagenesis Kit (Agilent Technologies, Santa Clara, Calif), according to the manufacturer's instructions. An N-terminal myc-tagged pCMV-Tag3A vector (211173; Agilent Technologies) containing the *MAP3K14* gene and the following mutagenic primers designed with Agilent QuikChange Primer Design program NIKMutF (5'-tgggcaaactggccgtgtgtagacagccag-3') and NIKMutR (5'-ctggctgtctacacggccagtttgccca-3') were used. Successful mutagenesis was confirmed by means of plasmid DNA sequencing at Eton Bioscience. One day before transfection, 500,000 HEK293T cells were seeded per well of a 6-well plate in antibiotic-free medium. Transfections were carried out with TransIT-LT1 Transfection Reagent (Mirus, Madison, Wis) according to the manufacturer's protocol. Cells were transfected with 1 μg of NIK^{myc} or mutated NIK^{myc} plasmid DNA. After 20 hours, cells were harvested and used in immunoblotting, as described below.

Western blot analysis
Lysates of fibroblasts and HEK293-transfected T cells were resolved by means of SDS-PAGE, transferred to nitrocellulose membranes, and probed with primary antibodies against p100/p52 (Cell Signaling, Danvers, Mass; 4882S), phospho p100 (Cell Signaling, 4810S), Myc (Cell Signaling, 2276S), NIK (Abcam, Cambridge, United Kingdom; ab137671), and β-actin (Cell Signaling, 4970S) according to standard protocols. Immunoblots were scanned in iBright FL1000 Imaging System (Invitrogen, Thermo Fisher Scientific, Carlsbad, Calif) and quantitatively analyzed using the ImageJ analyzer software (1.48v).

Scintillography
One mCi technetium 99 sulfur colloid was administered in 4 intradermal injections, 2 in the dorsum of each foot. Planar images from a gamma camera were acquired of the lower extremities and abdomen.

Statistical analysis
All data are presented as mean $\pm$ SEM, and compared using the unpaired Student t test for single comparisons and 2-way ANOVA for multiple comparisons. Statistical analysis was performed using GraphPad Prism software (San Diego, Calif).

REFERENCE

E1. Hoyos-Bachiloglu R, Chou J, Sodroski CN, Beano A, Bainter W, Angelova M, et al. A digenic human immunodeficiency characterized by IFNAR1 and IFNGR2 mutations. J Clin Invest 2017;127:4415-20.
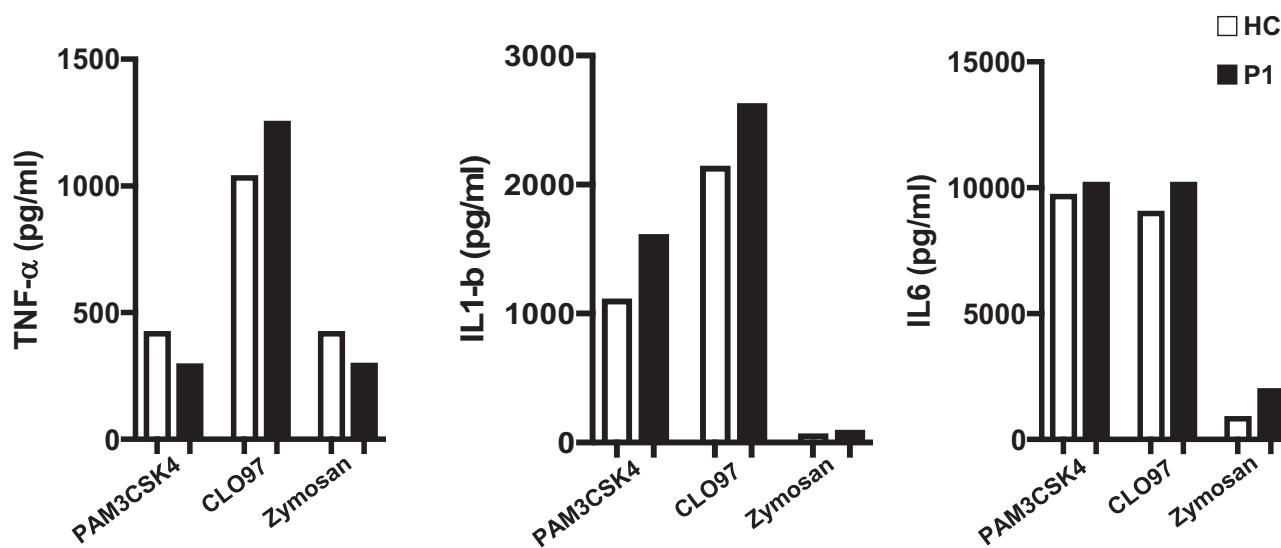
FIG E1. TLR responses in patient P1. TNF-α, IL1β, and IL-6 production in healthy control (HC) and P1 PBMCs after stimulation with PAM3CSK4 (TLR1/2), CLO97 (TLR7/8), and zymosan (TLR2/6) done by a commercial laboratory.
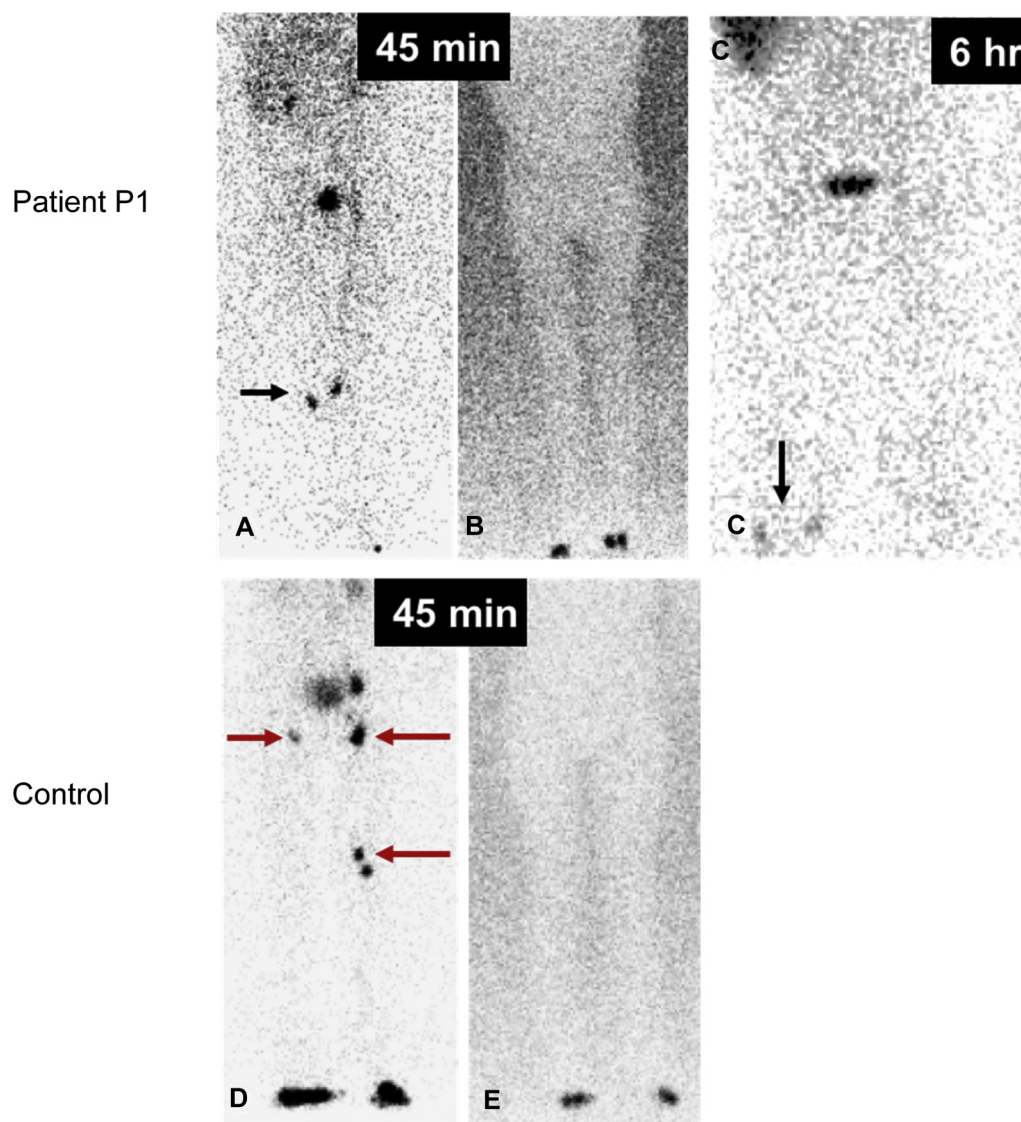
FIG E2. Lymphoscintigraphy of patient P1 and control. Anterior sweep **(A)**, transmission **(B)**, and planar **(C)** images from a lymphoscintigram of the bilateral lower extremities after intradermal injection of Technetium-99m sulfur colloid in the feet demonstrate no inguinal nodal transit up to 6 hours of imaging in P1. Two popliteal LNs (*black arrows*) were visualized throughout the study period. For comparison, a normal lymphoscintigram **(D** and **E)** in a 3-year-old male, with visualization of inguinal/pelvic LNs and left popliteal nodes (*red arrows*) within 45 minutes of injection. The visualization of popliteal nodes in lower extremity lymphoscintigraphy is variable, but was noted unilaterally in both the index and the comparison patient. Early systemic (liver/genitourinary) activity on both these examinations is in keeping with an incidental small amount of venous injection of the radiotracer. Transmission scans (images *B* and *E*) using Cobalt-57 flood source are used for anatomic localization.
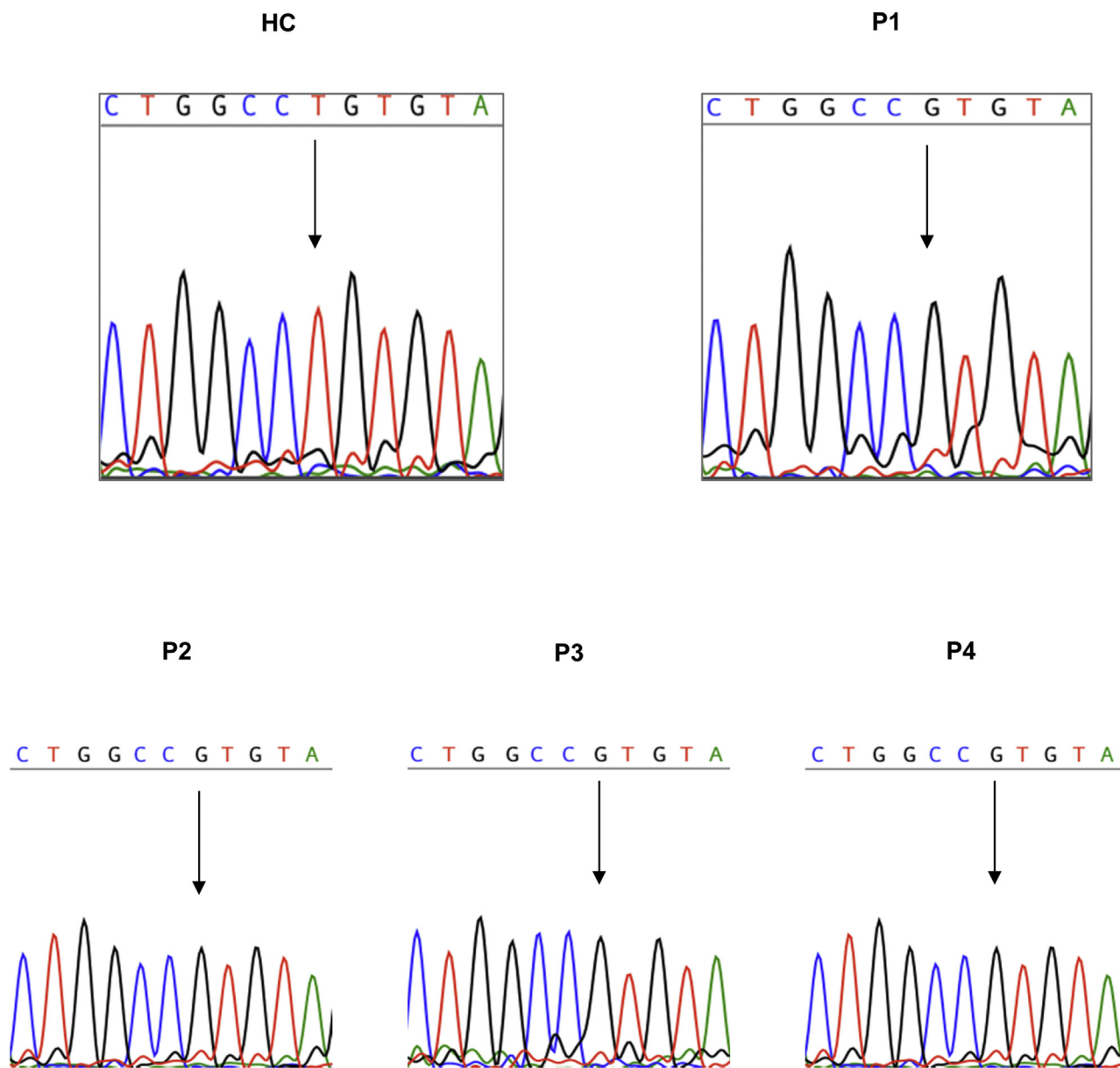
FIG E3. Sanger sequencing of the mutation. Results of sanger sequencing of the region surrounding the location of the mutation in *MAP3K14* (c.916delT) in a control, P1, P2, P3, and P4.